International Journal for Multidisciplinary Research (IJFMR)
E-ISSN: 2582-2160 ● Website: www.ijfmr.com ● Email: editor@ijfmr.com

Synthesis and Structural Elucidation of POM-Based Hybrid with A Common Cobalt Centre: It's Antibacterial Activity and Future Perspectives

***Rajarshi Chatterjee[1], *Arabinda Mandal[2]**

[1,2] Assistant Professor, Department of Chemistry, Bidhannagar College, Saltlake, Kolkata-64

Abstract

A novel hybrid Keggin tungstocobaltate $[Co(H_2O)_6][C_5H_6N]$ $H_4[CoW_{12}O_{40}][NO_3].3H_2O$ was prepared by the hydrothermal method and was characterized by elemental analyses, IR spectra, TG-DTA and single crystal X-ray diffraction techniques. This might be the first example of transition metal factionalized POM where the same cobalt metal resides at the centre of both of the cationic and anionic complexes. Furthermore, their antibacterial efficacy was determined by MIC and MBC on Gram-negative (Escherichia coli, Salmonella typhi) and Gram-positive (Streptococcus pneumoniae, Bacillus cereus) bacteria. The results indicated an acceptable bacteriostatic and bactericidal effects of this hybrid polyoxometalate.

Keywords: Polyoxometalates,crystal structure, Antibacterial activity, Gram-positive/negative bacteria

Introduction

For over two decades POMs have been intensively studied for their antibacterial activity against both Gram-positive and Gram-negative reference strains, and also against bacterial strains which are resistant to various antibiotics [1].The finding of new natural or chemically synthesized compounds with antibacterial activity [2] is a continuous challenge. As alternative chemotherapeutic agents, POMs have shown high antibacterial activities in creating new drugs to combat the antibiotic resistance of the bacteria. Studies at the interface of chemistry and biology are a prominent example of going beyond established areas of competence and thereby producing exciting new research results of the utmost importance. Recently, the study of the interactions between inorganic complexes and biomolecules is a prime target of multidisciplinary research. Due to the significant role of microorganisms in the development of various diseases and at the same time increasing antibiotic resistance following the excessive use of antibiotics, it is essential to find effective and new substances that have potent antibacterial impacts. That is why in recent years, antibacterial materials have found a special place to avoid the overuse of antibiotics. In this study, the antibacterial effects of our synthesized cobalto-POM on Escherichia coli, Salmonella typhi, Streptococcus pneumoniae and Bacillus cereus, were investigated due to their importance as human pathogens in nosocomial infection. Since 1970, when the inhibitory effect of the silicotungstic acid $H_4[SiW_{12}O_{40}]$ on murine leukemia and sarcoma viruses was discovered [3], the application of POMs in various biological systems has been a rapidly growing branch of science.

POMs were recently suggested as putative future drugs fighting against pathogenic bacteria[4].Polyoxometalates (POMs) have fascinated generations of chemists since the mid-18th-century, and they continue to attract promising young scientists all over the world. Their manifold structures and properties have been the focus of interdisciplinary research laboratories. Moreover, polyoxometalates excel through outstanding compositional and structural diversity, which enables fine-tuning of their electronic properties, redox properties, and chemical stability along with robustness for the design of future applied devices [5]. One popular tactic is to design and synthesize hybrid POM by incorporating transition metal-organic complexes with the POMs to form materials of multi property. [6] In this respect, the reaction system of functionalized hybrid POM under hydrothermal conditions is currently productive in isolating new polyoxometalates with novel structures and fulfilling certain properties [7].Due to their unique properties, POMs can be alternative chemotherapeutic agents instrumental in designing new antibiotics. In this research, we synthesized and characterized "smart" POM and validated their antibacterial effects in order to formulate and implement potential new drugs.

Experimental

Materials and Methods

Chemicals were readily available from commercial sources and were used as received without further purification. Na_2WO_4 (AR Loba, India), $Co(NO_3)_2.6H_2O$ (AR Loba, India), pyridine (Merck, India), were of reagent grade and were used as received. Deionized water was used as the solvent.

Synthesis of the complex $[Co(H_2O)_6][C_5H_6N]H_4[CoW_{12}O_{40}][NO_3].3H_2O$ (1)

The title compound was prepared by the hydrothermal method from a vigorously stirred as well as heated acidic mixture (acidified by adding 10 ml of 6(N) HNO_3) of 2.97 gm (9 mmol) $Na_2WO_4.2H_2O$ and 0.58 gm (2 mmol) $Co(NO_3)_2.6H_2O$ in 25 ml of water. The resulting pH was adjusted to 5 by adding drop wise 5 ml of pyridine. The entire mixture was then transferred into a Teflon jacket in PTTE- lined stainless steel pressure vessel and was kept in oven at 160^0C for consecutive five days under autogeneous pressure. The solution was cooled by decreasing temperature at a regular interval of 5^0C for one day. After cooling the autoclave to room temperature, green block shaped crystals were obtained, filtered, washed several times with distilled water and dried in air (yield 25% based on W). Composition of the complex was determined by elemental analysis: Found: C, 1.85; H, 0.88; N, 0.87; Co, 3.65; W, 67.49 % Calculated based on $C_5H_{28}Co_2N_2O_{52}W_{12}$: C, 1.83; H, 0.86; N, 0.86;; Co, 3.61; W, 67.42%. The following chemical reaction is expected.

$$2Co(NO_3)_2 + 12Na_2WO_4 + C_5H_5N + 21HNO_3 + H_2O = [Co(H_2O)_6][C_5H_6N]H_4[CoW_{12}O_{40}].NO_3.3H_2O + 24NaNO_3$$

Physical measurements

Elemental analyses were carried out using a Perkin–Elmer 240 elemental analyzer. The FTIR spectra of the compound were recorded as nujol mulls at ambient temperatures between the ranges 400–4000 cm^{-1}. The spectra were recorded on a Nicolet Magna IR 750 series-II FTIR spectrophotometer using KBr pellets. TG analyses were performed on a Perkin–Elmer Pyris Diamond TGA/DTA Analyzer instrument in flowing N_2 with a heating rate of 10^0C min^{-1}.

X-ray crystallography

X-ray diffraction data for **1** were collected at 298(2) K on a Bruker SMART APEX CCD X-ray diffractometer using graphite-monochromated MoKα radiation (λ = 0.71073Å). Determination of integrated intensities and cell refinement were performed with the SAINT [8]software package using a narrow-frame integration algorithm. An empirical absorption correction [9] (SADABS) was applied. The structure was solved by direct-methods with SHELXS-97 [10] and refined using full-matrix least-squares techniques against F^2 with anisotropic displacement parameters for non-hydrogen atoms with SHELXL-97 [11] except water molecules of crystallization. Hydrogen atoms (except waters of crystallization) were placed at calculated positions using suitable riding models with isotropic displacement parameters derived from their carrier atoms. In the final difference Fourier maps there were no remarkable peaks except the ghost peaks surrounding the tungsten atom and near disordered water molecules. A summary of crystal data and relevant refinement parameters for **1** is provided in Table 1. Selected bond distances and angles are given in Table 2.

Results and discussion

Molecular structure of $[Co(H_2O)_6][C_5H_6N]H_4[CoW_{12}O_{40}][NO_3]\ .3H_2O$ (1)

The crystal structure is composed of a Keggin-type $[CoW_{12}O_{40}]^{6-}$ anion, one hexa aqua cobalt $[Co(H_2O)_6]^{2+}$ counter cation and three water molecules of crystallization along with one NO_3^-group and one pyridinium ion $[C_5H_6N]^+$. The oxygen atom (O14) of the solvent water molecules in **1**, located near (1, 0, 1/6) was disordered between two centrosymmetrically related positions. $[CoW_{12}O_{40}]^{6-}$ consist of four vertex-sharing with trinuclear W_3O_{13} triads units each of which is made up of three edge-sharing WO_6 octahedra around the CoO_4 central tetrahedron (Fig. 1) [12].

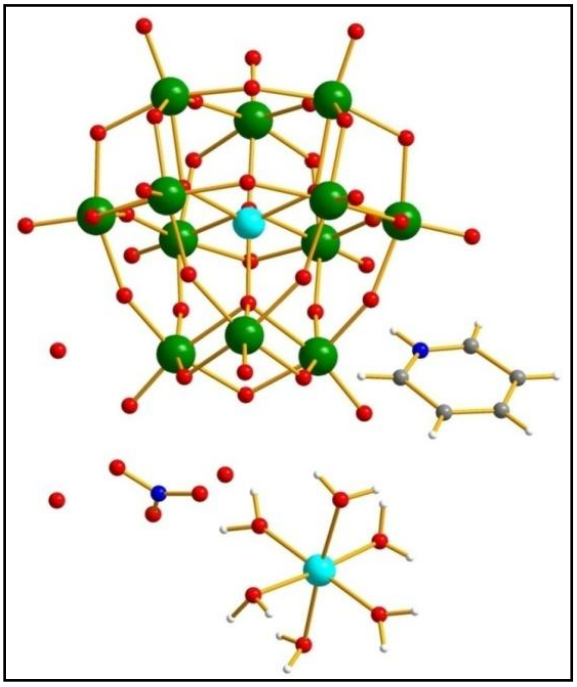

Fig-1(a). Ball-and-stick model of the complex $[Co(H_2O)_6][C_5H_6N]\ H_4[CoW_{12}O_{40}][NO_3].3H_2O$

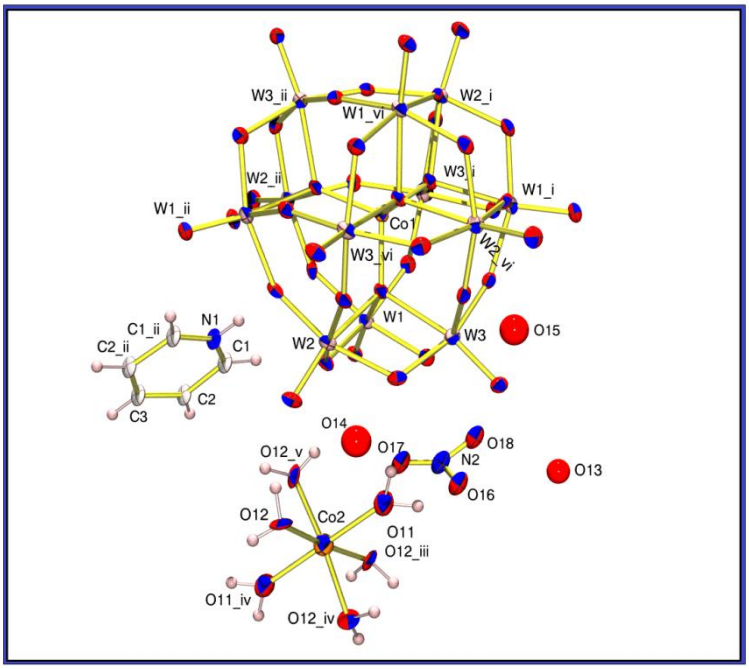

Fig-1(b).ORTEP diagram (30% ellipsoidal probability) with atom numbering scheme

[Symmetry codes: i=; ii=; iii=; iv= ; v=vi=]

According to the different coordination fashion of oxygen atoms in Keggin unit, the O atoms can be classified into three groups i.e. the unshared or terminal O atoms 'O_t', the bridging O atoms (O_b) connecting two W atoms, and the O atoms (O_c) of the central CoO_4. The W-O_t bond lengths vary between 1.66(2)- 1.73(2)Å, while the W-O_b, W-O_c bond distances lie in the range 1.88(2)-1.97(2) Å and 2.13(2)-2.20(2) Å, respectively. In the CoO_4 tetrahedron, the metal center (Co1) is seated at the intersection of three two-fold rotation axes with coordinates (½,0,0). The coordination geometry around the Co atom is distorted tetrahedral, which was reflected by central Co-O bond lengths [1.88(2) Å] and the O-Co-O angles [108.1(14) to 111.8(14)º. From the variations W-O distances and the bond angles around the W atoms it is evident that there is considerable distortion in the WO_6 octahedra in the complex. This is consistent with structural features of polyoxotungstates exhibiting Keggin structures [13-15].

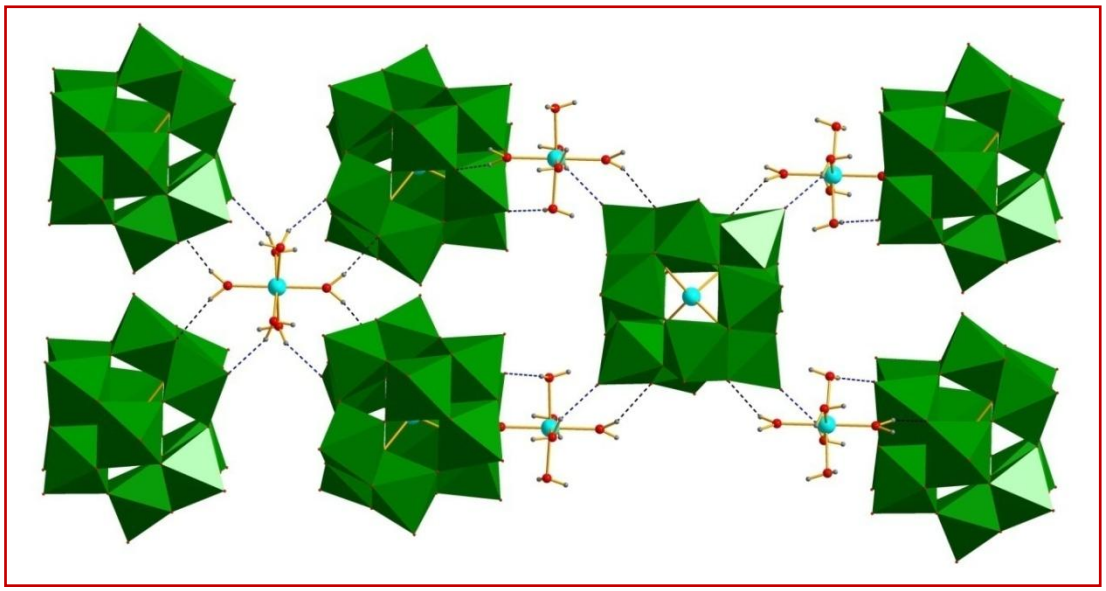

Fig-2. Combined polyhedral and ball-n-stick view of $[Co(H_2O)_6][C_5H_6N]$ $H_4[CoW_{12}O_{40}][NO_3].3H_2O$ in one-dimensional infinite chain propagating along the [001] direction,

Another part of the compound **1** is the presence of a discrete cobalt complex where the metal atom is surrounded by six molecules of water forming the cation. The Co atom is in a nearly regular octahedral coordination geometry, with Co-O distances between 1.99(4) and 2.07(4) Å, and angles ranging from 87.4(12) to 92.6(12)° are comparable with the reported values for related hexa aqua cobalt complexes. [16-17] Four oxygen atoms lying on the mirror plane, O12 and those generated by the symmetry operations (-x+2,-x+y+1,-z+1/3, x, x-y,-z+1/3, -x+2,-y+1,z), define the basal plane and the remaining two oxygen atoms, O11 and symmetry (-x+2,-x+y+1,-z+1/3) related oxygen atom, lying on the four-fold axis occupy the axial sites. The molecular structure of the complex reveals supramolecular frameworks by a combination of N-H…O, O-H…O and C-H…O hydrogen bonds [Table 3]. Intermolecular O11-H11…O6 (1-x, 1-y,z) and O12-H12…O3 (1-x, 1-y,z) hydrogen bonds link the hexa aqua cobalt cation and polyoxoanion to form an one-dimensional infinite chain propagating along the [001] direction, as shown in Fig-2. Centrosymmetrically related both cobalt octahedra and polyoxoanions tetrahedra are connected through pairs of O12-H12A…O4 (1-x, 1-x+y,1/3-z) hydrogen bonds, which according to graph-set notation [18-20] can be described as an $R_6^6(36)$ ring (Fig-3).

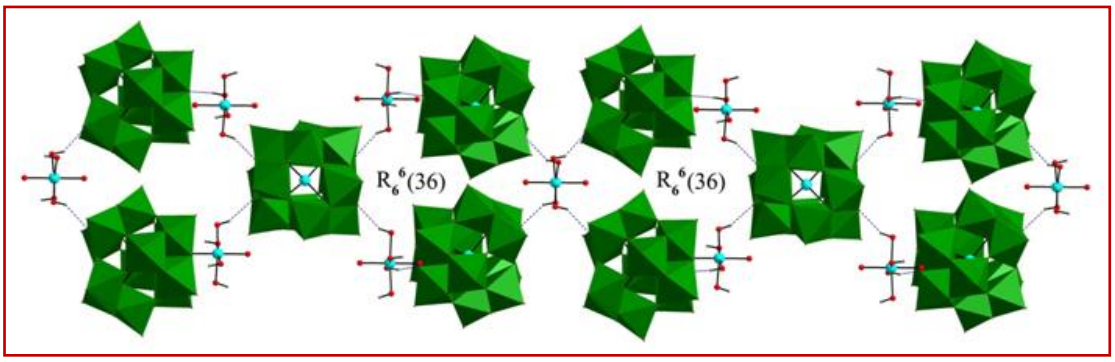

Fig-3. Combined polyhedral and ball-n-stick view of $[Co(H_2O)_6][C_5H_6N]$ $H_4[CoW_{12}O_{40}][NO_3].3H_2O$ ina $R_6^6(36)$ ring as per graph-set notation

It is to be pointed out that due to relatively larger size of the POM units than the hexaaquocobalt (II) units even after fusion of successive helices there remain inter-groove vacant space which accommodates pyridinium ions. Pyridinium ion acts as suitable H-donor for the Keggin terminal O acceptors simultaneously donating to four O atoms of the same Keggin POM unit that vertically landed on the center of the cap of the Keggin [Fig 5a, Table 3]. The tetrahedral hydrogen bonded network is a biporous network. The pyridinum ions also occupy the channels along the y-axis. Each pyridinium ion mainly interacts with strong tetra-furcated NH...O hydrogen bonding with the Keggin unit. Also it maintains bifurcated CH...O hydrogen bond with symmetry related adjacent Keggin units. Pyridinium ions also interact with $[Co(H_2O)_6]^{2+}$ units in a plane with Keggin units lying above and below this plane. (Fig-5b)

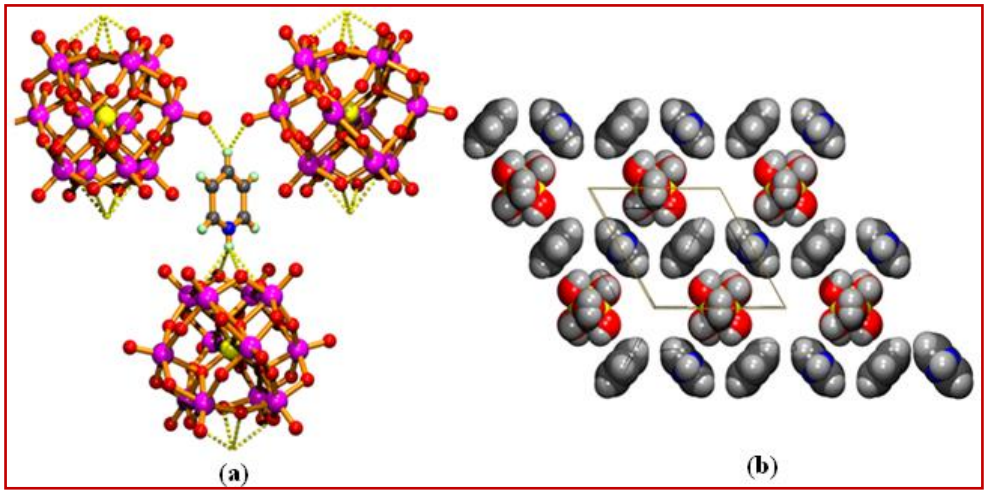

Fig-5 (a) The hydrogen bonded pyridinium ion. (b) Pyridinium ions and the hexa-aquo Co(II) units areorganized in a plane with Keggin units lying above and below this plane

Moreover, the title compound further forms a three-dimensional network by N-H…O and C-H…O hydrogen bonds between pyridinium ion and polyanion. The pyridinium ion also establishes bifurcated CH...O bond with two other Keggin unit on the other side leading to 2D supramolecular layers (Fig. 6).

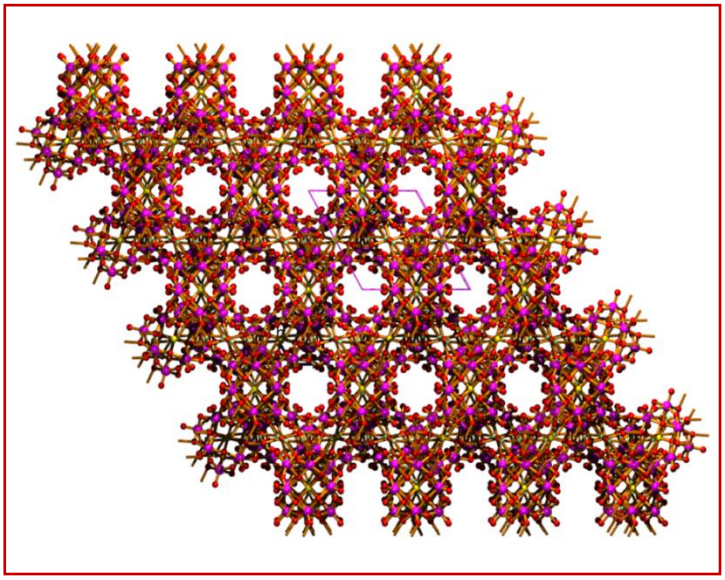

Fig- 6. The supramolecular assembly of POM and pyridinium ions.

Table 1

Crystal data and structure refinement parameters for (1)

Empirical formula	$C_5 H_{24}Co_2 N_2 O_{52} W_{12}$
Formula weight	3268.32
Temperature (K)	293(2)
Wavelength (Å)	0.71073
Crystal system	Hexagonal
Space group	$P6_222$
a, b, c(Å)	12.091(1), 12.091(1)), 33.296(8)
α, β,γ (°)	90.00 90.00 120.00(2)
Volume ($Å^3$)	4215.8(12)
Z	6
Calculated density (Mgm^{-3})	7.724
F(000)	8556
Limiting indices	$-11 \leq h \leq 11, -11 \leq k \leq 11, -31 \leq l \leq 32$
Reflections collected / unique	26077 / 1428 [R(int) = 0.1038]
Completeness to 2θ (%)	99.9
Refinement method	Full-matrix least-squares on F^2
Data / restraints / parameters	1428 / 121 / 208
Goodness-of-fit on F^2	1.207
Final R indices [I>2σ(I)]	$R_1 = 0.0518$, $wR_2 = 0.1324$
R indices (all data)	$R_1 = 0.0553$, $wR_2 = 0.1344$

Largest diff. peak and hole (eÅ^{-3})	1.742 and -1.243

Table 2
Selected bond lengths [Å] and angles (°) with esd's in parentheses for (1)

W(1)-O(10)	1.66(2)	W(2)-O(1)	2.13(2)
W(1)-O(2)	1.92(2)	W(3)-O(9)	1.68(2)
W(1)-O(4)	1.92(3)	W(3)-O(7)	1.89(2)
W(1)-O(7)#1	1.95(2)	W(3)-O(5)	1.90(2)
W(1)-O(8)	1.95(2)	W(3)-O(6)	1.91(2)
W(1)-O(1)	2.20(2)	W(3)-O(2)	1.97(2)
W(2)-O(3)	1.73(2)	W(3)-O(1)	2.17(2)
W(2)-O(8)#2	1.88(2)	Co(1)-O(1)	1.88(2)
W(2)-O(4)	1.91(2)	Co(2)-O(11)	1.99(4)
W(2)-O(5)#3	1.92(2)	Co(2)-O(12)	2.07(4)
W(2)-O(6)	1.95(3)	-----	----
O(1)#1-Co(1)-O(1)#2	108.1(14)	O(11)#4-Co(2)-O(12)#4	87.4(12)
O(1)-Co(1)-O(1)#1	111.8(14)	O(11)-Co(2)-O(12)#4	92.6(12)

Symmetry codes: #1 x-y,-y,-z #2 -x+1,-y,z #3 -x+y+1,y,-z #4 -x+2,-x+y+1,-z+1/3

Table 3
Intermolecular contacts of the compound (Å, °).

D—H···A	d(D—H)	d(H···A)	d(D···A)	D—H···A
N(1)—H(1)…O(4)^{i}	0.85	2.56	3.11(8)	123
N(1)—H(1)…O(8)^{i}	0.85	2.45	3.15(9)	141
O(11)—H(11)…O(6)^{ii}	0.87	2.26	3.08(4)	157
O(12)—H(12)…O(3)^{ii}	0.88	2.14	2.97(5)	158
O(12)—H(12A)…O(4)^{iii}	0.81	2.27	2.97(6)	145
C(3)—H(3)…O(9)^{iv}	0.93	2.28	3.00(5)	134

Symmetry codes: (i) x,x-y,1/3-z (ii) 1-x,1-y,z (iii) 1-x,1-x+y,1/3-z (iv) x-y,1-y,-z.
v) 1# (x- y,-y,-z) 2# (-x+1,-y,z) 3# (-x+y+1,y,-z) vi) 1# (-x+2,-x+y+1,-z+1/3) 2# (-x+2,-x+y+1,-z+1/3) 3# (x,x-y,-z+1/3) 4# (-x+2,-y+1,z)

Moreover as the cluster is neutral, it follows from the charge balance that the cobalt atom of both hexa aquo cobalt ion and cobalt atom of the CoO_4 tetrahedron in the Keggin polyoxoanion must prevail in +2 oxidation state. In order to confirm these valence-state attributions, bond valence sum (BVS) calculations [21] were performed for each cobalt, tungsten and oxygen center; On the basis of the charge balance, oxidation state of the central atom could be confidently located from bond valence sum (BVS) calculations. The working formula is BVS = Σ exp $[(r_0 - r) /B]$ where ris the observed bond distance and $r_0$and *B*are empirically determined parameters. r_0 = 1.921 Å for W^{6+}- O^{2-}, r_0 = 1.692 Å for Co^{2+}- O^{2-}, and *B* = 0.37 which is a constant. BVS values of tungsten in the polyoxo moiety listed in Table 4a, 4b and 4c, i.e. for W(1), W(2) and W(3) are 6.36, 6.32 and 6.48 respectively which gives an average value of 6.38 for the calculated oxidation state of W. The BVS values of cobalt (2.40) and tungsten (6.38) in

the polyoxoanion $[CoW_{12}O_{40}]^{6-}$ and cobalt (2.33) in $[Co(H_2O)_6]^{2+}$, listed in Table 4, Table 5 and Table 6 beautifully agreed with +2 valence state of cobalt and +6 valence state of tungsten in $[CoW_{12}O_{40}]^{6-}$ and +2 valence state of cobalt in $[Co(H_2O)_6]^{2+}$ respectively. In short, all the atoms fall within the expected bond valence limits. Besides this, charge balance considerations also dictate that in addition to the two protons associated with the tungsten core, there must be additional protonation site at the periphery of the polyoxo cluster. Valence sum calculations on the four triply bridging oxo-groups (W_3O) which line the cavity of the cluster provide oxygen valences of 1.5, clearly consistent with two protons delocalized over these sites. Consequently, the crystallographic data does not allow a definite assignment of the protonation site.

Table 4

Bond Valence Sums (BVS) for Tungsten Atoms in polyoxoanion $[CoW_{12}O_{40}]^{6-}$

(a)

Bond type	Bond	bond-dist	$[\exp[(r_0 - r)/B]$	BVS= Σ exp $[(r_0 - r)/B]$
Bridging	W(1)-O(1)	2.19	0.4833	
Bridging	W(1)-O(2)	1.92	1.0010	
Bridging	W(1)-O(4)	1.92	1.0010	
Bridging	W(1)-O(7)	1.95	0.9246	6.36
Bridging	W(1)-O(8)	1.95	0.9246	
Terminal	W(1)-O(10)	1.66	2.0247	

(b)

Bond type	Bond	bond-dist	$[\exp[(r_0 - r)/B]$	BVS= Σ exp $[(r_0 - r)/B]$
Bridging	W(2)-O(1)	2.13	0.5684	
Terminal	W(2)-O(3)	1.73	1.6757	
Bridging	W(2)-O(4)	1.91	1.0302	
Bridging	W(2)-O(5)	1.92	1.0010	6.32
Bridging	W(2)-O(6)	1.95	0.9246	
Bridging	W(2)-O(8)	1.88	1.1172	

(c)

Bond type	Bond	bond-dist	$[\exp[(r_0 - r)/B]$	BVS= Σ exp $[(r_0 - r)/B]$
Bridging	W(3)-O(1)	2.17	0.5102	
Bridging	W(3)-O(2)	1.97	0.8760	
Bridging	W(3)-O(5)	1.90	1.0584	
Bridging	W(3)-O(6)	1.91	1.0302	6.48
Bridging	W(3)-O(7)	1.89	1.0874	
Terminal	W(3)-O(9)	1.68	1.9181	

Table 5

Bond Valence Sums (BVS) for Cobalt Atom in polyoxoanion $[CoW_{12}O_{40}]^{6-}$				
Bond type	Bond	bond-dist	$[\exp[(r_0 - r)/B]$	BVS= $\Sigma \exp[(r_0 - r)/B]$
Central	Co(1)-O(1)	1. 88	0.6016	
Central	Co(1)-O(1)^1	1. 88	0.6016	2.40
Central	Co(1)-O(1)^2	1. 88	0.6016	
Central	Co(1)-O(1)^3	1. 88	0.6016	

Table 6

Bond Valence Sums (BVS) for Cobalt Atom in $[Co(H_2O)_6]^{2+}$ ion				
Bond type	Bond	bond-dist	$[\exp[(r_0 - r)/B]$	BVS= $\Sigma \exp[(r_0 - r)/B]$
Axial	Co(2)-O(11)	1.99	0.4469	
Axial	Co(2)-O(11)^1	1.99	0.4469	
Equatorial	Co(2)-O(12)	2.07	0.3600	
Equatorial	Co(2)-O(12)^2	2.07	0.3600	2.33
Equatorial	Co(2)-O(12)^3	2.07	0.3600	
Equatorial	Co(2)-O(12)^4	2.07	0.3600	

Vibrational Spectroscopy

The IR spectrum of the title compound has some characteristic bands for the polyoxoanion at 940.59, 877.84, 770 and 448.24 cm^{-1} which are attributed to ν (W=Ot terminal), ν (W–Ob-W octahedral edge sharing), ν (W–Oc-W octahedral corner sharing) and ν (Co–O tetrahedral), respectively [22] whereas for the pyridinium cation, bands have been observed at 684.82, 745.6, 1255.08, 1384.5, 1483.47, 1546.3, 1691.21, 3170 cm^{-1}. Features at 1255.08 cm^{-1} , 1483.47 cm^{-1} and 1691.21 cm^{-1} are attributed to stretching vibrations of (C–H), (C–C) and (C=N) bonds respectively. The ν (N-H) vibrations appear at 3170 cm^{-1} in the IR spectrum of $pyH.^+$ The ν (Co–O) of the discrete octahedral hexaaquo Co(II) cation is assigned at 502 cm^{-1}. In addition, a strong broad peak observed at 3570 cm^{-1} is assigned to ν (–OH) absorption along with the hydrogen bonds which proves the presence of lattice water. Comparing the IR spectra of $K_6[CoW_{12}O_{40}]$ the vibration frequencies of W–O bonds have shifted to lower wave numbers, showing the interaction of the polyoxoanions and cations as well as lattice water.

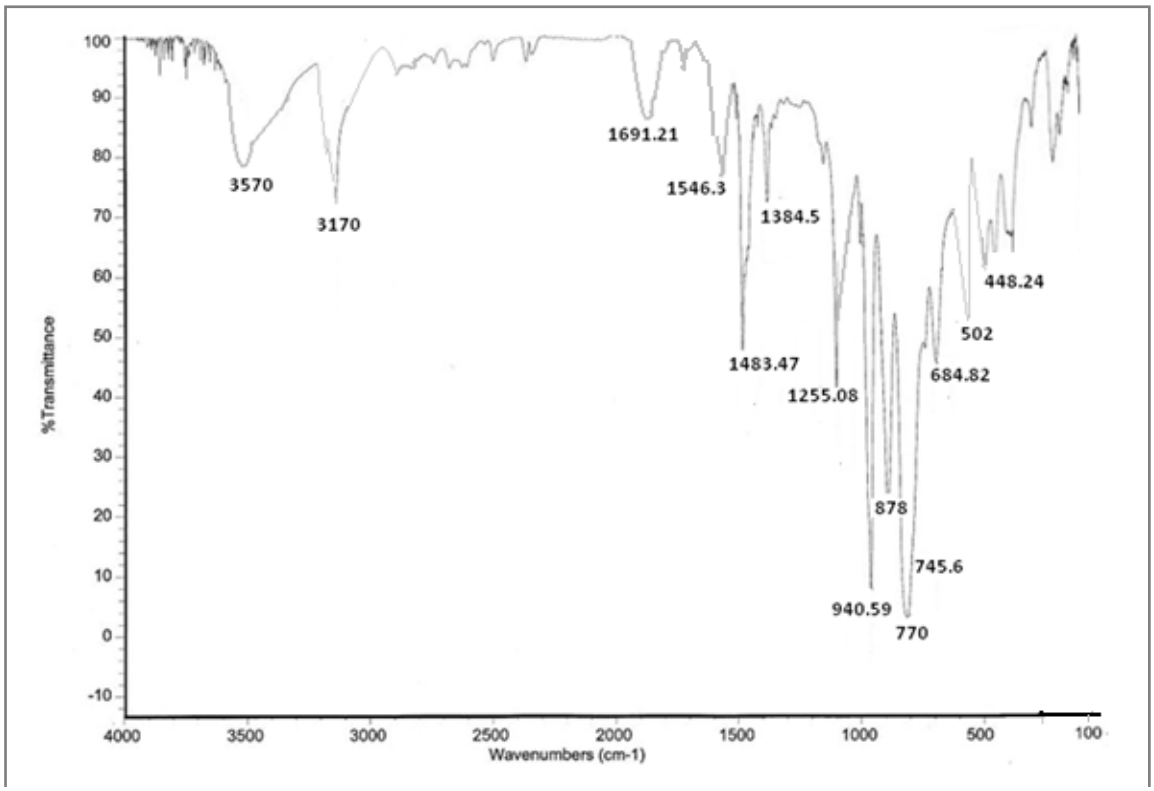

Fig-8. FTIR spectrum of $[Co(H_2O)_6][C_5H_6N]H_4[CoW_{12}O_{40}][NO_3].3H_2O$ taken as KBr pellet

Thermogravimetric analysis

The thermal decomposition profile (Fig. 7) of the title compound gives a total weight loss of 11.17% (calculated 10.92 %) in the range 40–575^{0}C.which agrees with the calculated weight loss of 11.10%. The thermal analysis curve can be divided into two stages. In the first stage, the weight loss of 3.56% (calculated 3.55%) in the range of 40–175^{0}C is attributed to the cumulative decomposition of three lattice water molecules and one NO_3^- ion. In the second stage, the weight loss of 7.61% (calculated 7.37%) in the range 175–410^{0}C corresponds to the overall decomposition of $[Co(H_2O)_6]^{2+}$ ion leading to the loss of $6H_2O$, pyridine, 3 water molecules coming from the reaction: $3H^+ + 5OH^- \rightarrow 5\ H_2O$ [one pyridinium H^+ and other two H^+ from the surface protons that are protonated externally). These are followed by two endothermic peaks at 128^{0}C and 290^{0}C respectively in the DTA curve. In addition, one exothermal peak at 563^{0}C in the later curve shows that the Keggin anion $[CoW_{12}O_{40}]^{6-}$ begins to decompose according to the following reaction.

$$2[CoW_{12}O_{40}]^{6-} \rightarrow Co_2O_3 + 24\ WO_3 + 5/2\ O_2$$

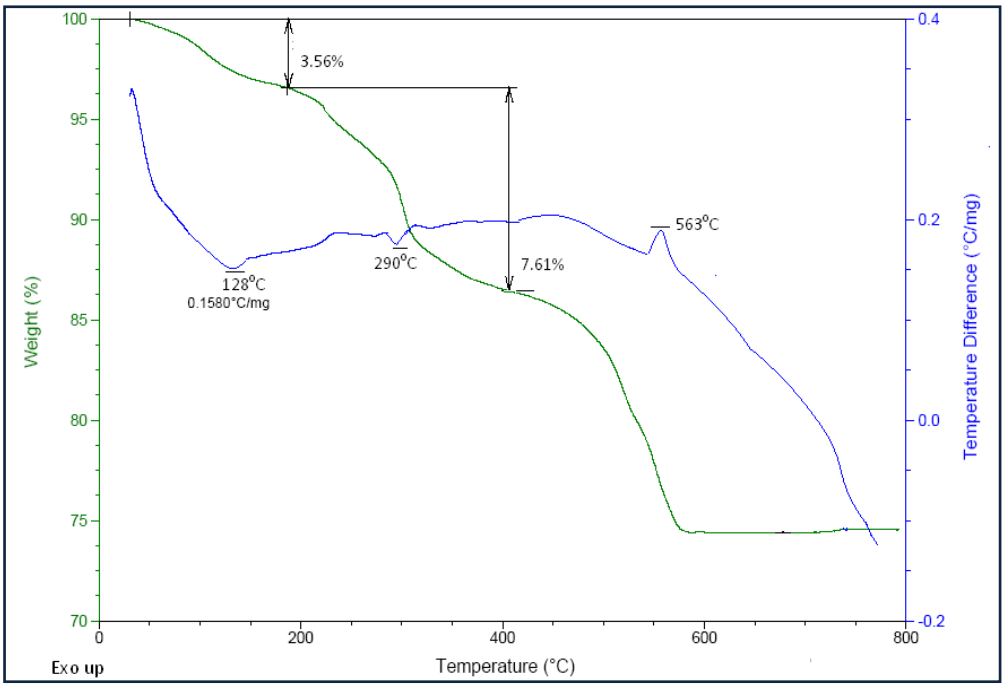

Fig-9. TGA of the complex $[Co(H_2O)_6][C_5H_6N]H_4[CoW_{12}O_{40}][NO_3].3H_2O$ in the range of 40–575^{0}C.

POM Pharmacology

All the isolated bacterial strains were achieved by colony formation on selective salt agar plates containing 6 mg/mL oxacillin. Four bacterial strains were tested in the antibacterial assays: Escherichia coli and Salmonella typhi as Gram-negative models, Streptococcus pneumoniae and Bacillus cereus as Gram-positive models. All bacterial strains were stored at −80°C and routinely grown at 40°C.

Antibacterial activity of compound (1)

Minimum Inhibitory Concentration (MIC)

In order to quantify the effectiveness, the Minimum Inhibitory Concentration (MIC)of this POMs on bacterial activity was determined using the broth microdilution method described by Quinn et al. [23], the Clinical and Laboratory Standards Institute [24], adapted for this experiment. Testing was conducted on the same Gram-negative and Gram-positive bacteria. Suspensions of microorganisms in saline buffer (NaCl solution 0.15 M) obtained were inoculated. The diluted POM solution in nutrient broth (Merck KGaA, Darmstadt, Germany) was prepared and an amount of 2.5 mg/well of active POM were placed in sterile micro plate. The micro plate thus prepared was incubated at 37 ± 2 °C for 24 h. Comparisons of the amount of bacterial growth in well containing POM solution with the amount of growth in the growth-control well was performed and the maximal dilution for which the tested POMs inhibited bacterial growth was established. The Gram-positive bacterial cell wall is composed of a thick, multilayered peptidoglycan sheath outside of the cytoplasmic membrane, while the Gram-negative cell wall is composed of an outer membrane linked by lipoproteins to thin, mainly single-layered peptidoglycan. The peptidoglycan is located within the periplasmic space that is created between the outer and inner membranes. It therefore follows that the most sensitive microorganism was Gram-positive *Bacillus cereus*, with a MIC value of 0.02 mg/mL, while the MIC of POM-1 against pathogenic

bacteria B. cereus, was equal to 0.56 mg/mL. The Gram-negative bacteria E.coliwas more resistant to POM-1 both possessed MICs corresponding to 0.22mg/ mL. Such differences in MIC between the Gram-negative and Gram-positive bacteria suggest that the mechanism of action of the POM-1 may involve damage to the cell membrane [25].

Minimum Bactericidal Concentration (MBC)

The minimum bactericidal activity (Minimum Bactericidal Concentration) of POM for the four bacterial species mentioned above was established using the microdilution method. 5 µL of POM solutions from the well where the inhibitory effect was observed were introduced in the same nutrient broth as mentioned above and inoculations on nutrient agar sterile plates (Merck KGaA, Darmstadt, Germany) were performed for similar dilutions. The plate thus prepared was incubated for 24 h at 37 ± 2 °C and bacterial growth was observed. The reading of the results was performed at 24 h by observing the evolution of the bacterial growth on the solid medium.Polyoxometalates aresaid to be bactericidal if they prevent growth on this medium. The minimum bactericidal concentration was determined for the lowest dilution at which bacterial growth was blocked. The cumulative MIC and MBC data is given below in a tabular form.

Table7. Concentration of active POM against bacteria

Bacteria	MIC (mg/ml)	MBC (mg/ml)
Escherichia coli	0.22	0.45
Salmonella typhi	0.24	0.48
Streptococcus pneumoniae	0.44	0.72
Bacillus cereus	0.56	0.86

Conclusions

A novel inorganic-organic hybrid compound composed of Keggin tungstocobaltate has been synthesized by hydrothermal method in one-pot reaction by interaction of the composing elements without the need for any polyoxoanion precursor species and its crystal structure was solved by single crystal x-ray diffraction techniques. The bioactivity of polyoxometalates has been known for many years but still has large space to explore. The synthesized POM possesses higher antibacterial activity against the Gram-positive strains compared with the Gram-negative strains, suggesting that the mechanism of action is linked to the structure of the bacterial cell wall. The results of this work on the antibacterial activity of polyoxometalates show that antibacterial activity of the compounds is more relative with their component element than with anionic structure, need further investigations.

References

1. BernoldH. (2005) Front. Biosci.10:275
2. Vică M.L., Glevitzky I. (2021) Antibiotics.10: 689
3. Chermann J. C., Raynaud M., Jasmin C. (1970) Nature 227: 173
4. Chen X., Yan S., Wang H. (2015) Carbohydr. Polym.117:673
5. Sullens T.A., Jensen R. A., Shvareva T. Y. (2004) J. Am. Chem. Soc. 126: 2676
6. Wang Y., Li H., Yang Y., Shi L. (2013) Angew. Chem. Int. Ed17: 4577

7. Muller A., Das S. K., Kogerler P., Bogge H. (2006) Angew. Chem. Int. Ed. 44: 741
8. Brandenburg K. (1999) DIAMOND Crystal Impact GbR, Bonn, Germany.
9. Niu J. Y., Wang Z. L., Wang J. P. (2004) Polyhedron. 23: 773
10. Liu K., Meng F-X., Chen Y-G. (2007) Trans Met Chem. 32: 350
11. Sha J., Peng J., Chen J., Liu H., Tian A. (2007) Solid State Sci. 9: 1019
12. Fleck M., Bohaty L. (2006) Acta Cryst. C62: m26
13. Genther D. J., Squattrito P.J., Yearley E.J., Pinkerton A. (2007) Acta Cryst. C63: m604
14. Zhong H., Xie H-L., Luo C-J. (1995) Angew. Chem. Int. Ed. Engl. 34: 1555
15. Wang X., Qin C., Wang E., Li Y., Hao N., Xu L. (2004) Inorg. Chem., 43: 1850
16. BreseN.E.,Keeffe M.O.(1991) Acta Crystallogr.B47: 192
17. Brown I. D., Altermatt D. (1985) Acta Crystallogr. B41: 244
18. Nomiya K., Miwa M., Kobayash R., Aiso M. (1981) Bull. Chem. Soc. Jpn. 54: 2983.
19. Bruker (2007) APEX2, SAINT and XPREP. Bruker AXS Inc., Madison, Wisconsin, USA.
20. Bruker (2001) SADABS. Bruker AXS Inc., Madison, Wisconsin, USA.
21. Sheldrick G. M. (2008) Acta Cryst. A64: 112
22. Anderson O.P. (1972) J Chem Soc Dalton Trans 2597
23. Quinn P.J., Markey B.K. (2011) Veterinary Microbiology and Microbial Disease. Wiley, USA
24. Clinical and Laboratory Standards Institute (CLSI). Wayne, NJ, USA: 2018. pp. 15–53
25. Enderle A.G., Castillo I-F.,,Blasco E.A., Mitchell S.G. (2022) Appl. Polym. Mater. 4: 4144